ARTICLE

Low Temperature Critical Growth of High Quality Nitrogen Doped Graphene on Dielectrics by Plasma-Enhanced Chemical Vapor Deposition

Dacheng Wei,[*,†,‡,§] Lan Peng,[†,‡] Menglin Li,[†,‡] Hongying Mao,[∥] Tianchao Niu,[∥] Cheng Han,[§] Wei Chen,[§,∥] and Andrew Thye Shen Wee[§]

[†]Department of Macromolecular Science, Fudan University, Shanghai 200433, China, [‡]State Key Laboratory of Molecular Engineering of Polymers, Fudan University, Shanghai 200433, China, [§]Physics Department, National University of Singapore, 2 Science Drive 3, Singapore 117542, Singapore, and [∥]Chemistry Department, National University of Singapore, 3 Science Drive 3, Singapore 117543, Singapore

ABSTRACT Nitrogen doping is one of the most promising routes to modulate the electronic characteristic of graphene. Plasma-enhanced chemical vapor depostion (PECVD) enables low-temperature graphene growth. However, PECVD growth of nitrogen doped graphene (NG) usually requires metal-catalysts, and to the best of our knowledge, only amorphous carbon—nitrogen films have been produced on dielectric surfaces by metal-free PECVD. Here, a critical factor for metal-free PECVD growth of NG is reported, which allows high quality NG crystals to be grown directly on dielectrics like SiO_2/Si, Al_2O_3, h-BN, mica at 435 °C without a catalyst. Thus, the processes needed for loading the samples on dielectrics and n-type doping are realized in a simple PECVD, which would be of significance for future graphene electronics due to its compatibility with the current microelectronic processes.

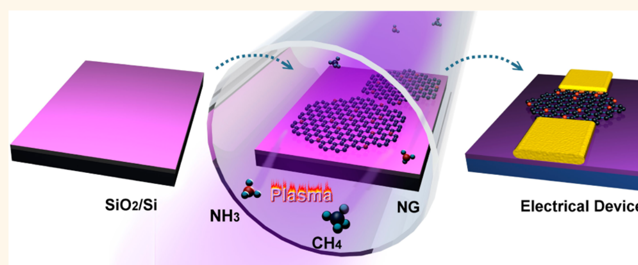

KEYWORDS: chemical vapor deposition · doping · graphene · nanomaterials · scanning probe microscopy

For usage in electronics, the growth process must be capable of modulating the graphene to be p-type or n-type.[1−3] Both theoretical and experimental studies have shown that nitrogen doping is an effective route toward this goal.[3−5] Nitrogen atoms release extra electrons into graphene, shifting the Fermi level into the valence band to provide an n-type extrinsic electrical conductivity. Moreover, the nitrogen substitution disrupts the ideal sp^2 hybridization of the graphene lattice, thus locally inducing significant changes to its electronic properties and chemical reactivity, which gives rise to potential applications[2] in electronics devices,[4,5] electrochemical biosensors,[6] electrocatalysis,[7] spintronics,[8] and so on. As the first step toward these applications, a nitrogen doping process with corresponding compatibility is required. To date, methods,[3] such as metal-catalytic chemical vapor deposition (CVD),[4] arc-discharge,[9] and postsynthesis treatment including NH_3 plasma,[6] Joule[5] or thermal[10] heating in NH_3, have been reported to produce nitrogen doped graphene (NG). However, a method to directly grow NG on dielectrics is still lacking, and for practical applications in electronics, the existing growth methods suffer from impurities, wrinkles and breakage of the NG samples introduced in the postgrowth transfer process commonly used.

To solve this problem, plasma-enhanced CVD (PECVD) is particularly attractive, since the high energy plasma environment enables low-temperature growth of carbon materials on metals, or even directly on dielectric surfaces.[11−17] Several groups have demonstrated direct growth of pristine graphene (p-G) on dielectric substrates by PECVD.[18,19] Recently, we realized the efficient crystal growth of p-G on dielectric substrates by introducing H_2 plasma in a PECVD process.[20] In the case of nitrogen doped samples, previous studies have demonstrated

* Address correspondence to weidc@fudan.edu.cn.

Received for review March 26, 2014 and accepted December 31, 2014.

Published online January 12, 2015
10.1021/nn505214f

© 2015 American Chemical Society

the use of (CH_4 + NH_3 or N_2) PECVD to produce nitrogen doped nanotubes[14−16] or NG[11−13] in the presence of metal catalysts. Thus far, to the best of our knowledge, only amorphous carbon−nitrogen films have been produced on the dielectric surface by PECVD without metal catalysts.[21−23] In this article, we observe the competitive processes of nucleation and etching of NG in PECVD, and demonstrate that efficient crystal growth of NG only takes place at a critical equilibrium state between these competitive processes. On the basis of this finding, we develop a critical PECVD (c-PECVD) method, which realizes metal-free growth of high quality hexagonal NG crystals or continuous NG films with atomically clean surfaces directly on SiO_2/Si, Al_2O_3, hexagonal boron nitride (h-BN), mica, highly oriented pyrolytic graphite (HOPG) substrates at temperatures as low as 435 °C.

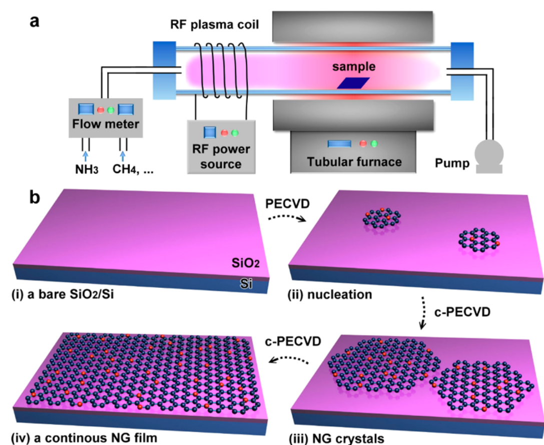

Figure 1. Schematic illustrations of (a) the PECVD system used for growth of NG and (b) the growth procedure.

RESULTS AND DISCUSSION

Figure 1 illustrates a typical procedure for the c-PECVD growth of NG on SiO_2/Si. The procedure consists of the nucleation of CN_x clusters, followed by critical crystal growth of NG from these clusters. A clean SiO_2/Si substrate was placed in the center of a quartz tube mounted inside a homemade remote radiofrequency (13.56 MHz) PECVD system. After CH_4 + NH_3 (30% NH_3, 46 mTorr) plasma CVD at 700 °C for 8 min, small discrete graphitic CN_x clusters were deposited on the SiO_2/Si substrate, and the height profile shows that most of the nucleated clusters were lower than 1 nm, indicating the monolayer nature of the clusters (Figure 2a). In the next stage, the clusters were used as the seeds, and the temperature was decreased to 650 °C. After CH_4 + NH_3 (30% NH_3, 46 mTorr) plasma CVD for 100 min, both scanning electron microscopy (SEM, Figure S1) and atomic force microscopy (AFM, Figure 2b, Supporting Information Figure S2) images

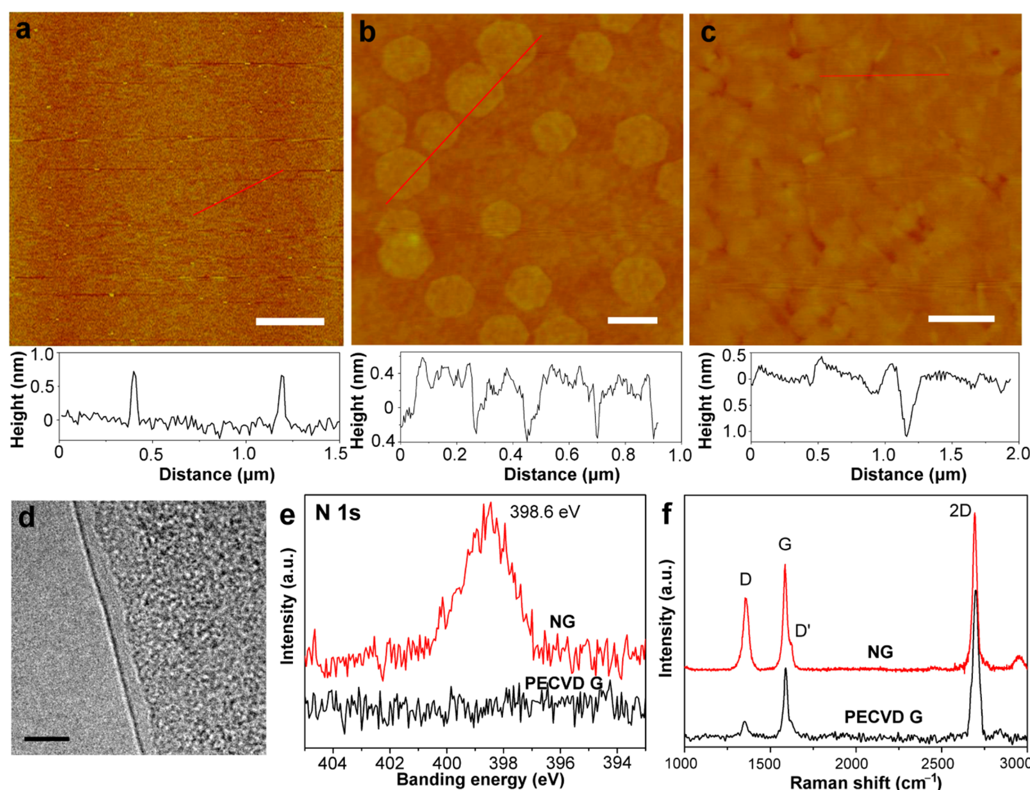

Figure 2. (a−c) AFM images of (a) the graphitic CN_x clusters after nucleation at 700 °C for 8 min, (b) hexagonal NG crystals after c-PECVD at 650 °C for 100 min, and (c) a continuous NG film on SiO_2/Si. The bottom insets are the height profiles across the red lines in the AFM images. (d) TEM image of a monolayer NG sample. (e) N 1s XPS and (f) Raman spectra of NG and the pristine graphene produced by PECVD. The scale bars are 1 μm (a and c), 200 nm (b), 5 nm (d).

show that hexagonal crystals were grown on the whole surface of SiO_2/Si. These structures exist in very high yield and with relatively narrow size distribution ranging from 100 to 400 nm. All edges are straight, and the angles between adjacent edges are 120°. The height profile reveals that most samples have monolayer structures. With a higher seed density (700 °C, 15 min) and a longer growth time (650 °C, 180 min), neighboring domains merged, resulting in a continuous membrane fully covering the SiO_2/Si substrate (Figure 2c). Normally, an atomically flat planar surface is expected to be inevitably necessary for preparing graphene on various substrates.[24] Our results show that even the amorphous and slightly rough nature of the SiO_2/Si surface does not prevent the growth of NG crystals into a continuous film. After growth, the NG film was transferred to copper grids. The transmission electron microscopy (TEM, Figure 2d) cross-sectional image displays a clear single layer structure, indicating that the NG samples produced here are predominantly monolayered.

X-ray photoelectron spectroscopy (XPS) measurement (Figure S3) confirms the presence of nitrogen in NG. A control p-G sample was synthesized by a similar PECVD process without introducing NH_3 for the nitrogen doping (see Experimental Section and ref 20 for details). The C 1s peaks of both samples are located at 284.6 eV, indicating that most carbon atoms are arranged in a conjugated honeycomb lattice. The N 1s peak is only detected in NG. The main peak (Figure 2e) is located at 398.6 eV, suggesting that the nitrogen atoms are bonded mainly in "pyridinic" N form (nitrogen atom has two carbon neighbors in a hexagonal ring).[4] Figure 2f shows representative Raman spectra of NG and p-G grown on SiO_2/Si by c-PECVD. The intensity maps of the D, G and 2D bands reveal good uniformity of the NG sample (Supporting Information Figure S4). The narrow, symmetric shape and high intensity of the 2D band (Figure 2f, Supporting Information Figure S4) confirm the monolayer nature of both samples.[25] Unlike the p-G spectrum, the NG spectrum has an obvious D' band, which is attributed to the defect-induced intravalley double resonance scattering process,[26] and a remarkably increased D-band, which is attributed to elastically scattered photoexcited electrons created by the large number of nitrogen atoms embedded in the graphene lattice before emitting a phonon.[4,27] Owing to the shifting of the Fermi level caused by nitrogen doping, the intensity ratio of the G to 2D peak decreases, consistent with previously reported results.[26,28] Moreover, all Raman spectra were collected under ambient conditions. Due to the exposure in air during the measurement, absorbed oxygen or water molecules have doped the p-G into p-type, giving rise to an upshift of the G band (1589 cm^{-1}) and the 2D band (2698 cm^{-1}) from the neutrality point (G band, 1584 cm^{-1}; 2D band, 2685 cm^{-1}). In the case of the NG, the G band and 2D band downshift to 1586 and 2693 cm^{-1}, compared with p-G, respectively. Although the NG still shows weak p-type behavior, the downshift of both the G band and the 2D band confirms the electron doping of graphene by nitrogen atoms.[28]

Besides SiO_2/Si, other inert surfaces can also be used as growth substrates in c-PECVD, such as Al_2O_3 (Supporting Information Figure S5), h-BN (Supporting Information Figure S6), mica (Supporting Information Figure S7), *etc.* For scanning tunnelling microscope (STM) studies, the NG samples (Supporting Information Figure S8) were prepared by c-PECVD on HOPG, because the HOPG provides an inert surface for metal-free growth, and it is conductive and atomically flat for STM analysis. Representative STM images of NG (Figure 3) indicate that the samples have a well-defined crystalline structure with an atomically clean surface. The edges (Figure 3e) are atomically smooth, and the complicated edge patterns are attributed to the scattering[29] and interference[30] of electronic wave functions on the edge nitrogen or the nonuniform edge structures. We observed features similar to the CVD NG reported previously,[26,27] which display a clear graphitic lattice decorated with several bright nitrogen-dopant defects (Figure 3a,b). The presence of nitrogen-dopants leads to significant changes in the local density of states (DOS) of graphene, which are identified by scanning tunnelling spectroscopy (STS). Around the nitrogen dopant, the most prominent feature of the STS spectrum (Figure 3c) is an obvious depression of the curve at about 0.4 eV. The depression occurs near the Dirac point where the DOS of graphene is low.[27,31] The suppression of the local DOS below the Fermi level results in a large electron−hole asymmetry around the N atoms, thus a higher contrast of the nitrogen dopants in the STM image (Supporting Information Figure S9) is observed when a negative tip bias is applied. STS spectra taken at the positions around the nitrogen-dopant, 1 nm away, and in the pristine region reveal that the Dirac point is located at about 0.4, 0.3, and 0 eV, respectively, indicating a strong electron doping effect of graphene from the embedded nitrogen-dopant atoms.[26,27]

Controlled experiments show that the growth of NG strongly depends on the NH_3 content and the growth temperature (Figure 3d). When the experimental parameters are located in the purple regions of Figure 3d (low temperature, high NH_3 content), nothing can be grown on the SiO_2/Si; whereas at the opposite reaction parameters located in the orange regions of Figure 3d (high temperature, low NH_3 content), large amount of graphitic CN_x clusters (Supporting Information Figure S10) are nucleated, covering the whole surface of the SiO_2/Si substrate. The parameters for crystal growth of NG are located in very narrow regions marked in green color between them, indicating

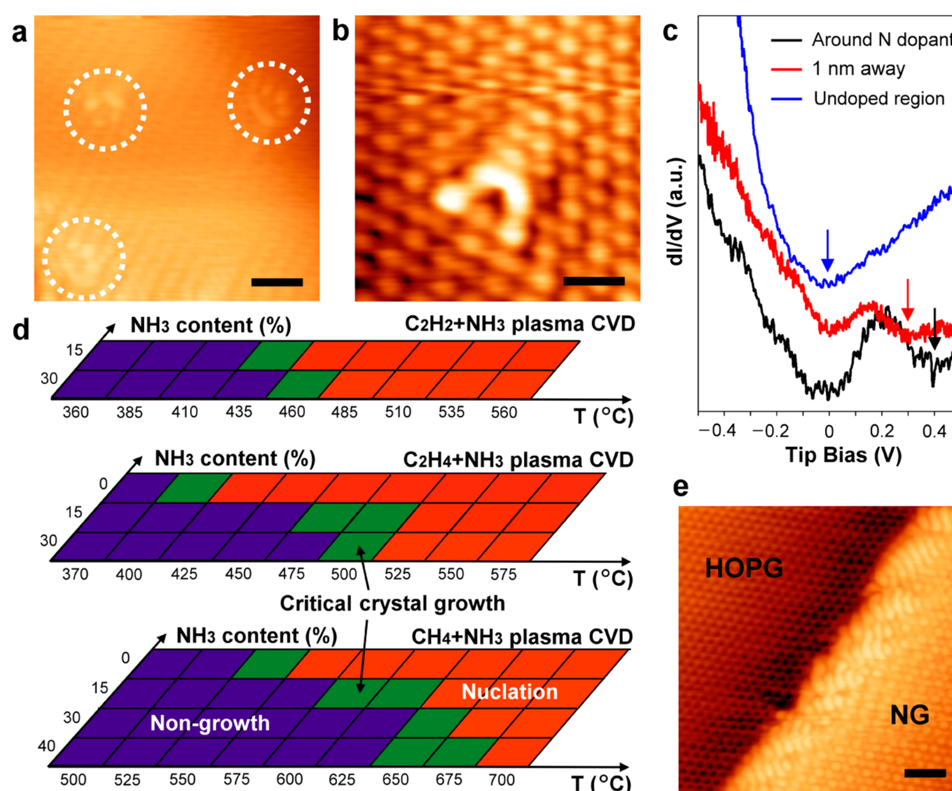

Figure 3. (a and b) STM images and (c) STS spectra of NG grown on HOPG. Dashed circles in (a) indicate the nitrogen dopants, and (b) is the enlarged image of the upper-left dopant in (a). The arrows in (c) indicate the positions of Dirac point. (d) Plots of the experimental results as a function of the temperature (*T*) and the NH_3 content using different carbon precursor gases. Crystal growth of NG only takes place under critical parameters indicated in green color. (e) STM image of the edge of NG grown on HOPG. The scale bars are 1 nm (a and e), 0.5 nm (b).

that the crystal growth only takes place at a critical temperature (T_c) lower than that required for CN_x cluster nucleation and higher than that for nongrowth, and the T_c decreases when the NH_3 content decreases. This result implies competitive processes exist in the c-PECVD growth of NG. The plasma decomposes precursor molecules into highly reactive C_xH_y species (radicals, ions, atoms) as the feedstock for graphene growth at low temperature,[11−17] while the NH_3 plasma generates nitrogen-containing species for substitutional incorporation of nitrogen atoms into the graphene lattice. Reactive C_xH_y species and nitrogen-containing species result in nucleation of graphitic CN_x clusters at a temperature higher than T_c, and introduce structural defects on the edges, which prevent the growth of NG crystals. Thus, amorphous carbon−nitrogen films were typically grown by metal-free PECVD.[21−23] On the other hand, atomic hydrogen is commonly accepted as an etchant during carbon growth.[32] In our previous work, we observed an etching effect of graphene from the edges by H_2 plasma in CH_4+H_2 PECVD, demonstrating that the H_2 plasma can remove growth defects from the edges, keep the edges active for efficient growth of graphene crystals on dielectrics.[20] Other groups found that NH_3 plasma was a more effective source of atomic hydrogen compared with H_2 plasma.[14−16] NH_3 plasma can selectively etch amorphous carbon contamination, thus largely promoting the growth of carbon nanotubes or fibers in a NH_3+CH_4 PECVD process.[14−16] Here, the moderate etching effect of the NH_3 plasma suppresses the nucleation of graphitic clusters and removes edge defects, keeping the edges active and atomically smooth (Figure 3e) during the whole growth process. Therefore, in a critical equilibrium between the competitive processes of the CH_4 plasma and the NH_3 plasma, efficient crystal growth of NG is realized at temperatures as low as 600 °C on a dielectric surface. If we use other precursor molecules with lower hydrogen content, such as C_2H_4 or C_2H_2, lower atomic hydrogen concentration will be generated from the precursor molecules, and as a result, the critical equilibrium occurs at a lower temperature. Therefore, when C_2H_4 or C_2H_2 is used as the carbon source, T_c can be further reduced to as low as 475 °C (Supporting Information Figure S11) or 435 °C (Supporting Information Figure S12), respectively, when the NH_3 content is 15%, as shown in Figure 3d.

For practical applications in electronics, modulation doping is usually required to produce single-crystalline nanostructure junctions. As an example, graphene p−n junctions, which combine p-G and NG in a seamless crystalline structure, have been produced by controllable supply of the nitrogen precursor in a copper-catalyzed CVD process, and this nanostructure has

potential applications in high-efficiency optoelectronic and electronic devices.[33] With the use of metal-free c-PECVD, modulated nitrogen doping can be realized at lower temperatures. Figure 4a shows a sample produced by the two stage c-PECVD process. In the initial stage, NG crystals were grown by c-PECVD on the SiO_2/Si substrate, and these NG crystals were directly used as the seeds for continued c-PECVD growth of p-G in the second stage. Due to differences in electrical characteristics, different contrasts were observed in the SEM image.[33,34] The dark islands correspond to graphene grains doped with nitrogen atoms, which are surrounded by brighter p-G regions. By reversed process, we produced crystals with p-G cores and NG shells (Figure 4b), indicating the high controllability of nitrogen doping by c-PECVD.

We fabricated field-effect transistors (FETs) of NG, in which the growth substrate (SiO_2/Si) was directly used as the dielectric and the bottom gate (Figure 5a). To obtain the intrinsic properties, the devices were current-annealed and then measured in high vacuum (7×10^{-8} mbar) at room temperature.[5] Figure 5b shows the typical output characteristics (drain current *versus* source drain voltage) of a NG device. The symmetrical linear behavior indicates an ohmic contact between the electrodes and NG. The drain current increases with increasing gate voltage, and the transfer curves of eight NG FETs (Figure 5c) show the Dirac points at negative gate voltages ($-15 \sim -30$ V), indicating a typical n-type behavior, consistent with previous reported results.[4,5] For comparison, FETs of pristine PECVD graphene on SiO_2/Si were fabricated and analyzed under the same conditions. Transfer curves (Supporting Information Figure S13) show a suppression of the electron transport branch, and this electron–hole asymmetry originates from imbalanced carrier injection from the electrodes caused by misalignment of the electrode and channel neutrality points.[35,36] The Dirac points shifted positively to 10–30 V, which indicates that p-G exhibits p-type behavior. Besides the dopants, the charge transfer between graphene and substrates can also induce a doping to graphene. For instance, when a graphene absorbs on the SiO_2 surface through van der Waals interactions, the inhomogeneous topology of the amorphous SiO_2 surface promotes a total charge density displacement on the absorbed graphene sheet, giving rise to electron-rich as well as hole-rich regions on the graphene.[37] The adsorbed graphene sheet exhibits a net total charge density gain. A significant surface state density of SiO_2 just below the conduction band edge donates electrons to the graphene to balance the chemical potential at the interface,[37,38] and as a result, Romero *et al.* found n-type behavior of graphene on SiO_2/Si substrates after long-term degassing of the device in

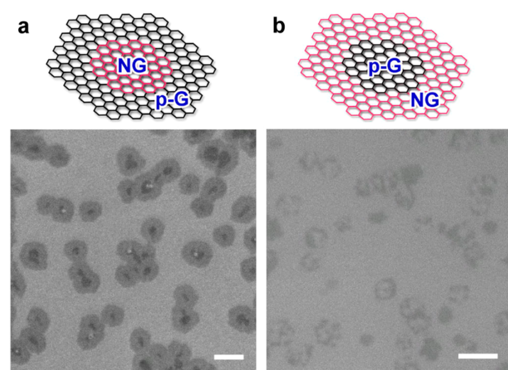

Figure 4. SEM images of graphene crystals on SiO_2/Si with NG core and p-G shell (a) and with p-G core and NG shell (b). The upper insets are the schematic drawings of the modulation doped graphene crystals. The scale bars are 300 nm.

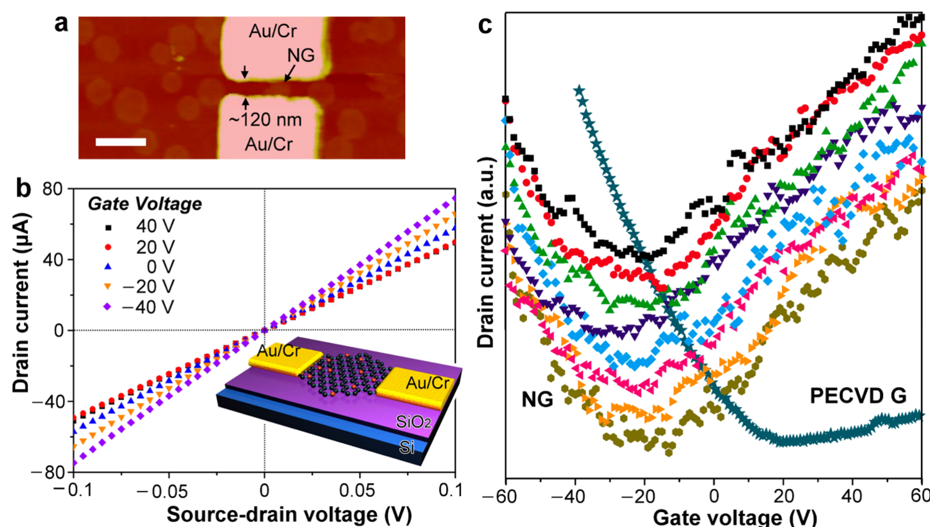

Figure 5. (a) AFM image of a device of NG. The scale bar is 500 nm. (b) Output characteristics of the NG device at various gate voltages. The inset is schematic of the device configuration. (c) Transfer characteristics (source drain voltage at 0.02 V) of eight FET devices of NG and a FET device of pristine graphene produced by PECVD.

vacuum at 200 °C.[39] Moreover, n-type or p-type doping of graphene, lying on the SiO_2 substrate, can be tuned through suitable graphene/SiO_2 "interface engineering".[40,41] In our case, the SiO_2 surface was passivated and terminated by hydrogen or hydrocarbons after growth of the p-G or NG samples by $H_2 + CH_4$ or $NH_3 + CH_4$ PECVD,[42] and such a surface causes a hole doping of graphene.[36,41] Therefore, the p-type behavior of p-G is attributed to the doping effect from hydrogen passivated substrates as well as the Au/Cr contact,[43] and the n-type behavior of NG originates from the nitrogen dopants, but not from the substrate underneath.

Calculated FET mobilities of NG are in the range of 100−400 $cm^2\ V^{-1}\ s^{-1}$, and we believe that the mobilities can be further improved by using boron nitride[44] or other modified surfaces[38,41] to reduce amount of charged impurities trapped in the SiO_2 surface,[45] or using other metals to improve the carrier injection from the electrodes.[46,47] The mobilities are higher than those of amorphous carbon−nitrogen films (10 $cm^2\ V^{-1}\ s^{-1}$) produced by metal-free PECVD,[21,22] and comparable to those of NG (200−450 $cm^2\ V^{-1}\ s^{-1}$) produced by metal-catalytic CVD,[4] indicating the high quality of our samples for electronic applications. For comparison, we transferred the NG samples to other SiO_2/Si substrates using poly methyl-methacrylate.[48] Defects and impurities were observed from SEM images (Supporting Information Figure S14), and electrical measurement (Supporting Information Figure S15) of the transferred NG showed a decrease in mobility to about 32 $cm^2\ V^{-1}\ s^{-1}$, indicating the importance of the direct growth technology in producing high performance graphene devices.

CONCLUSION

In summary, we have developed a low-temperature c-PECVD process to produce monolayer NG directly on amorphous insulating SiO_2/Si surface, and also on Al_2O_3, h-BN, mica, HOPG substrate. The growth temperature reaches as low as 435 °C, when C_2H_2 is used as the carbon source in c-PECVD. To our knowledge, this is the lowest reported temperature for growing NG crystals; thus, this method can decrease the energy consumption and cost for industrial-scale production, as well as be compatible with silicon CMOS fabrication processes. STM and electrical-transport measurements show that nitrogen doping can effectively modulate the electrical properties of graphene, and reveal that the samples have high quality, even though no metal catalysts are employed during the growth. This, as well as the atomically clean surface, and the metal-free growth process allows NG samples to be directly incorporated into high performance electrical devices, avoiding the inconvenient postgrowth transfer process commonly used. We believe this method would be of significant value in future graphene electronics due to its compatibility with the current microelectronic processes.

EXPERIMENTAL SECTION

Growth of Nitrogen Doped Graphene. To obtain a clean surface, a SiO_2/Si substrate was annealed in H_2 (50 mTorr) at 1000 °C for 15 min. Other low temperature processes can also be used to clean the surface, such as argon plasma treatment, or annealing the substrate in vacuum at 400 °C for 5 h. The cleaned substrate was placed in the center of a tubular furnace (MTI Corporation, OTF-1200X). In the first step, the furnace was heated to 700 °C, and then $NH_3 + CH_4$ plasma (30% NH_3, 46 mTorr) was generated upstream by a remote radio frequency plasma generator (K-Mate, VERG-500, 80 W). After 8 min, graphitic CN_x clusters nucleated on the SiO_2/Si substrate. In the second step, the clusters were used as the seeds for crystal growth of NG in $NH_3 + CH_4$ plasma CVD (30% NH_3, 46 mTorr), and the temperature was decreased to 650 °C. The growth lasted for 100 min. Finally, the furnace was cooled to room temperature under ambient H_2. NG crystals were obtained on the surface of the SiO_2/Si substrate. To grow p-G, graphitic clusters were nucleated on a clean SiO_2/Si substrate by $CH_4 + H_2$ plasma CVD (30% H_2, 48 mTorr) at 650 °C for 5 min, and then the graphitic clusters were used as seeds for growth of p-G crystals by CH_4+H_2 plasma CVD (30% H_2, 48 mTorr) at 600 °C for 90 min.[20]

Modulation Doping. To produce crystals with NG core and p-G shell, a clean SiO_2/Si substrate was annealed and placed in the center of the furnace. The furnace was heated to 700 °C, and then $NH_3 + CH_4$ plasma (30% NH_3, 46 mTorr) was generated upstream. After 8 min, graphitic CN_x clusters were nucleated on the SiO_2/Si substrate. The temperature was decreased to 650 °C, and the c-PECVD growth (30% NH_3, 46 mTorr) of NG proceeded for 60 min. After that, NH_3 was turned off, and c-PECVD growth of p-G continued using NG as the seeds in $H_2 + CH_4$ plasma (30% H_2, 48 mTorr) CVD at 600 °C. After 60 min growth, the furnace was cooled to room temperature under ambient H_2.

Characterization. The samples were measured by AFM (Veeco D3000, tapping mode), Raman (Renishaw 2000, 514 nm), field emission SEM (JEOL JSM-6700F), field emission TEM (JEOL 2010F, acceleration voltage: 200 kV), respectively. For TEM measurement, the sample was transferred to TEM grids by poly methyl-methacrylate (PMMA). The PMMA was removed by acetone vapor, and then the sample was annealed at 300 °C for 20 min in Ar (99.999%) at 200 mTorr. XPS measurements were carried out in ESCA-lab system with an Al Kα source (1486.6 eV). The base pressure is better than 1×10^{-10} mbar. STM measurements were carried out in a custom-built multichamber ultrahigh vacuum system housing an Omicron LT-STM in the analysis chamber with a base pressure better than 1.0×10^{-10} mbar. All the STM images were recorded in constant current mode at liquid nitrogen temperature (77 K) using electrochemically etched tungsten (W) tips. The STS data were acquired using a lock-in amplifier by applying a small sinusoidal modulation to the tip bias voltage (typically 30 mV at 600 Hz). All STM images were processed using WSxM.[49]

Device Fabrication and Electrical Measurement. The source-drain electrodes (5/50 nm Cr/Au) were patterned on the sample by electron beam lithography and thermal deposition. To obtain a better contact, thermal annealing was performed in an Ar atomsphere at 250 °C for 30 min using a tube furnace. For electrical measurements, both the Au/Cr electrodes and the p++ Si back gate were wire bonded using Al wires. Before measurement, the device was current-annealed in vacuum (7×10^{-8} mbar) by applying a bias cycled between −2 and 2 V for at least 5 min to completely remove the absorbed molecules. The electrical characterization was carried out by a semiconductor

analyzer (Agilent B2912A) in vacuum (7×10^{-8} mbar) at room temperature.

Conflict of Interest: The authors declare no competing financial interest.

Supporting Information Available: Supplementary figures S1–S15. This material is available free of charge *via* the Internet at http://pubs.acs.org.

Acknowledgment. This work was supported by Lee Kuan Yew Post Doctoral Fellowship Grant (R-144-000-263-112), Singapore MOE AcRF Tier 1 Grant (R-144-000-321-112) and National Program for Thousand Young Talents of China. D.W. designed research and supervised the project. D.W., L.P., and M. L. prepared the sample and did AFM, SEM, TEM measurement. H.M. measured XPS. D.W. and T.N. measured STM and STS. D.W. did the electron beam lithography. H.C. and C.W. did the metal deposition, D.W., H.C., C.W. measured the devices.

REFERENCES AND NOTES

1. Wei, D.; Wu, B.; Guo, Y.; Yu, G.; Liu, Y. Controllable Chemical Vapor Deposition Growth of Few Layer Graphene for Electronic Devices. *Acc. Chem. Res.* **2013**, *46*, 106–115.
2. Wei, D.; Liu, Y. Controllable Synthesis of Graphene and Its Applications. *Adv. Mater.* **2010**, *22*, 3225–3241.
3. Wang, H.; Maiyalagan, T.; Wang, X. Review on Recent Progress in Nitrogen-Doped Graphene: Synthesis, Characterization, and Its Potential Applications. *ACS Catal.* **2012**, *2*, 781–794.
4. Wei, D.; Liu, Y.; Wang, Y.; Zhang, H.; Huang, L.; Yu, G. Synthesis of N-Doped Graphene by Chemical Vapor Deposition and Its Electrical Properties. *Nano Lett.* **2009**, *9*, 1752–1758.
5. Wang, X. R.; Li, X. L.; Zhang, L.; Yoon, Y. K.; Weber, P. K.; Wan, H. L.; Guo, J.; Dai, H. J. N-Doping of Graphene Through Electrothermal Reactions with Ammonia. *Science* **2009**, *324*, 768–771.
6. Wang, Y.; Shao, Y. Y.; Matson, D. W.; Li, J. H.; Lin, Y. H. Nitrogen-Doped Graphene and Its Application in Electrochemical Biosensing. *ACS Nano* **2010**, *4*, 1790–1798.
7. Qu, L. T.; Liu, Y.; Baek, J. B.; Dai, L. M. Nitrogen-Doped Graphene as Efficient Metal-Free Electrocatalyst for Oxygen Reduction in Fuel Cells. *ACS Nano* **2010**, *4*, 1321–1326.
8. Li, Y.; Zhou, Z.; Shen, P.; Chen, Z. Spin Gapless Semiconductor-Metal-Half metal Properties in Nitrogen-Doped Zigzag Graphene Nanoribbons. *ACS Nano* **2009**, *3*, 1952–1958.
9. Subrahmanyam, K. S.; Panchakarla, L. S.; Govindaraj, A.; Rao, C. N. R. Simple Method of Preparing Graphene Flakes by an Arc-Discharge Method. *J. Phys. Chem. C* **2009**, *113*, 4257–4259.
10. Li, X. L.; Wang, H. L.; Robinson, J. T.; Sanchez, H.; Diankov, G.; Dai, H. J. Simultaneous Nitrogen Doping and Reduction of Graphene Oxide. *J. Am. Chem. Soc.* **2009**, *131*, 15939–15944.
11. Terasawa, T.; Saiki, K. Synthesis of Nitrogen-Doped Graphene by Plasma-Enhanced Chemical Vapor Deposition. *Jpn. J. Appl. Phys.* **2012**, *51*, 055101.
12. Wang, C. D.; Yuen, M. F.; Ng, T. W.; Jha, S. K.; Lu, Z. Z.; Kwok, S. Y.; Wong, T. L.; Yang, X.; Lee, C. S.; Lee, S. T.; Zhang, W. J. Plasma-Assisted Growth and Nitrogen Doping of Graphene Films. *Appl. Phys. Lett.* **2012**, *100*, 253107.
13. Kumar, A.; Voevodin, A. A.; Paul, R.; Altfeder, I.; Zemlyanov, D.; Zakharov, D. N.; Fisher, T. S. Nitrogen-Doped Graphene by Microwave Plasma Chemical Vapor Deposition. *Thin Solid Films* **2013**, *528*, 269–273.
14. Wong, W. K.; Li, C. P.; Au, F. C. K.; Fung, M. K.; Sun, X. H.; Lee, C. S.; Lee, S. T.; Zhu, W. Fabrication and Characterization of Pure and Well-Aligned Carbon Nanotubes Using Methane/Nitrogen–Ammonia Plasma. *J. Phys. Chem. B* **2003**, *107*, 1514–1517.
15. Bell, M. S.; Lacerda, R. G.; Teo, K. B. K.; Rupesinghe, N. L.; Amaratunga, G. A. J.; Milne, W. I.; Chhowalla, M. Plasma Composition During Plasma-Enhanced Chemical Vapor Deposition of Carbon Nanotubes. *Appl. Phys. Lett.* **2004**, *85*, 1137–1139.
16. Lee, D. H.; Lee, W. J.; Kim, S. O. Highly Efficient Vertical Growth of Wall-Number-Selected, N-Doped Carbon Nanotube Arrays. *Nano Lett.* **2009**, *9*, 1427–1432.
17. Li, Y.; Mann, D.; Rolandi, M.; Kim, W.; Ural, A.; Hung, S.; Javey, A.; Cao, J.; Wang, D.; Dai, H.; *et al.* Preferential Growth of Semiconducting Single-Walled Carbon Nanotubes by a Plasma Enhanced CVD Method. *Nano Lett.* **2004**, *4*, 317–321.
18. Zhang, L.; Shi, Z.; Wang, Y.; Yang, R.; Shi, D.; Zhang, G. Catalyst-Free Growth of Nanographene Films on Various Substrates. *Nano Res.* **2011**, *4*, 315–321.
19. Malesevic, A.; Vitchev, R.; Schouteden, K.; Volodin, A.; Zhang, L.; Tendeloo, G. V.; Vanhulsel, A.; Haesendonck, C. V. Synthesis of Few-Layer Graphene *via* Microwave Plasma-Enhanced Chemical Vapour Deposition. *Nanotechnology* **2008**, *19*, 305604.
20. Wei, D.; Lu, Y.; Han, C.; Niu, T.; Chen, W.; Wee, A. T. S. Critical Crystal Growth of Graphene on Dielectric Substrates at Low Temperature for Electronic Devices. *Angew. Chem., Int. Ed.* **2013**, *52*, 14121–14126.
21. Schwan, J.; Batori, V.; Ulrich, S.; Ehrhardt, H.; Silva, S. R. P. Nitrogen Doping of Amorphous Carbon Thin Films. *J. Appl. Phys.* **1998**, *84*, 2071.
22. Freire, F. L., Jr.; Franceschini, D. F. Structure and Mechanical Properties of Hard Amorphous Carbon-Nitrogen Films Obtained by Plasma Decomposition of Methane-Ammonia Mixtures. *Thin Solid Films* **1997**, *293*, 236–243.
23. Hsueh, H.-C.; Li, H.-C.; Chiang, D.; Lee, S. Effects of Ammonia/Methane Mixtures on Characteristics of Plasma Enhanced Chemical Vapor Deposition n-Type Carbon Films. *J. Electrochem. Soc.* **2012**, *159*, D77–D83.
24. Kim, K.; Lee, C.; Choi, J. Catalyst-Free Direct Growth of Triangular Nano-Graphene on All Substrates. *J. Phys. Chem. C* **2011**, *115*, 14488–14493.
25. Ferrari, A. C.; Meyer, J. C.; Scardaci, V.; Casiraghi, C.; Lazzeri, M.; Mauri, F.; Piscanec, S.; Jiang, D.; Novoselov, K. S.; Roth, S.; Geim, A. K. Raman Spectrum of Graphene and Graphene Layers. *Phys. Rev. Lett.* **2006**, *97*, 187401.
26. Lv, R.; Qing, L.; Botello-Mendez, A. R.; Hayashi, T.; Wang, B.; Berkdemir, A.; Hao, Q.; Elias, A. L.; Cruz-Silva, R.; Gutierrez, H. R.; *et al.* Nitrogen-Doped graphene: Beyond Single Substitution and Enhanced Molecular Sensing. *Sci. Rep.* **2012**, *2*, 586.
27. Zhao, L.; He, R.; Rim, K. T.; Schiros, T.; Kim, K. S.; Zhou, H.; Gutierrez, C.; Chockalingam, S. P.; Arguello, C. J.; Pálová, L.; *et al.* Visualizing Individual Nitrogen Dopants in Monolayer Graphene. *Science* **2011**, *333*, 999–1003.
28. Das, A.; Pisana, S.; Chakraborty, B.; Piscanec, S.; Saha, S. K.; Waghmare, U. V.; Novoselov, K. S.; Krishnamurthy, H. R.; Geim, A. K.; Ferrari, A. C.; *et al.* Monitoring Dopants by Raman Scattering in An Electrochemically Top-Gated Graphene Transistor. *Nat. Nanotechnol.* **2008**, *3*, 210–215.
29. Niimi, Y.; Matsui, T.; Kambara, H.; Tagami, K.; Tsukada, M.; Fukuyama, H. Scanning Tunnelling Microscopy and Spectroscopy of the Electronic Local Density of States of Graphite Surfaces Near Monoatomic Step Edges. *Phys. Rev. B* **2006**, *73*, 085421.
30. Yang, H.; Mayne, A.; Boucherit, M.; Comtet, G.; Dujardin, G.; Kuk, Y. Quantum Interference Channeling at Graphene Edges. *Nano Lett.* **2010**, *10*, 943–947.
31. Zhang, Y.; Brar, V. W.; Wang, F.; Girit, C.; Yayon, Y.; Panlasigui, M.; Zettl, A.; Crommie, M. F. Giant Phonon-Induced Conductance in Scanning Tunnelling Spectroscopy of Gate-Tunable Graphene. *Nat. Phys.* **2008**, *4*, 627–630.
32. Xie, L. M.; Jiao, L. Y.; Dai, H. J. Selective Etching of Graphene Edges by Hydrogen Plasma. *J. Am. Chem. Soc.* **2010**, *132*, 14751–14753.
33. Yan, K.; Wu, D.; Peng, H.; Jin, L.; Fu, Q.; Bao, X.; Liu, Z. Modulation-Doped Growth of Mosaic Graphene with Single-Crystalline p-n Junctions for Efficient Photocurrent Generation. *Nat. Commun.* **2012**, *3*, 1280.
34. Wei, D.; Xie, L.; Lee, K. K.; Hu, Z.; Tan, S.; Chen, W.; Sow, C. H.; Chen, K.; Liu, Y.; Wee, A. T. S. Controllable Unzipping for

Intramolecular Junctions of Graphene Nanoribbons and Single-Walled Carbon Nanotubes. *Nat. Commun.* **2013**, *4*, 1374.

35. Farmer, D. B.; Golizadeh-Mojarad, R.; Perebeinos, V.; Lin, Y. M.; Tulevski, G. S.; Tsang, J. C.; Avouris, P. Chemical Doping and Electron-Hole Conduction Asymmetry in Graphene Devices. *Nano Lett.* **2009**, *9*, 388–392.
36. Liu, W.; Wei, J.; Sun, X.; Yu, H. A Study on Graphene-Metal Contact. *Crystals* **2013**, *3*, 257–274.
37. Miwa, R. H.; Schmidt, T. M.; Scopel, W. L.; Fazzio, A. Doping of Graphene Adsorbed on The a-SiO_2 Surface. *Appl. Phys. Lett.* **2011**, *99*, 163108.
38. Fan, X. F.; Zheng, W. T.; Chihaia, V.; Shen, Z. X.; Kuo, J. L. Interaction Between Graphene and the Surface of SiO_2. *J. Phys.: Condens. Matter* **2012**, *24*, 305004.
39. Romero, H. E.; Shen, N.; Joshi, P.; Gutierrez, H. R.; Tadigadapa, S. A.; Sofo, J. O.; Eklund, P. C. n-Type Behavior of Graphene Supported on Si/SiO_2 Substrates. *ACS Nano* **2008**, *2*, 2037–2044.
40. Wang, R.; Wang, S.; Zhang, D.; Li, Z.; Fang, Y.; Qiu, X. Control of Carrier Type and Density in Exfoliated Graphene by Interface Engineering. *ACS Nano* **2011**, *5*, 408–412.
41. Nagashio, K.; Yamashita, T.; Nishimura, T.; Kita, K.; Toriumi, A. Electrical Transport Properties of Graphene on SiO_2 with Specific Surface Structures. *J. Appl. Phys.* **2011**, *110*, 024513.
42. Gupta, V.; Madaan, N.; Jensen, D. S.; Kunzler, S. C.; Liford, M. R. Hydrogen Plasma Treatment of Silicon Dioxide for Improved Silane Deposition. *Langmuir* **2013**, *29*, 3604–3609.
43. Giovannetti, G.; Khomyakov, P.; Brocks, G.; Karpan, V.; van den Brink, J.; Kelly, P. Doping Graphene with Metal Contacts. *Phys. Rev. Lett.* **2008**, *101*, 026803.
44. Abanin, D. A.; Morozov, S. V.; Ponomarenko, L. A.; Gorvachev, R. V.; Mayorov, A. S.; Katsnelson, M. I.; Watanabe, K.; Taniguchi, T.; Novoselov, K. S.; Levitov, L. S.; Geim, A. K. Giant Nonlocality Near the Dirac Point in Graphene. *Science* **2011**, *332*, 328–330.
45. Chen, J.; Jang, C.; Xiao, S.; Ishigami, M.; Fuharer, M. S. Intrinsic and Extrinsic Performance Limits of Graphene Devices on SiO_2. *Nat. Nanotechnol.* **2008**, *3*, 206–209.
46. Schwierz, F. Graphene Transistors. *Nat. Nanotechnol.* **2010**, *5*, 487–496.
47. Xia, F.; Perebeinos, V.; Lin, Y.; Wu, Y.; Avouris, P. The Origins and Limits of Metal-Graphene Junction Resistance. *Nat. Nanotechnol.* **2011**, *6*, 179–184.
48. Reina, A.; Son, H.; Jiao, L.; Fan, B.; Dresselhaus, M. S.; Liu, Z.; Kong, J. Transferring and Identification of Single- and Few-Layer Graphene on Arbitrary Substrates. *J. Phys. Chem. C* **2008**, *112*, 17741–17744.
49. Horcas, I.; Fernandez, R.; Gomez-Rodriguez, J. M.; Colchero, J.; Gomez-Herrero, J.; Baro, A. M. WSXM: A Software for Scanning Probe Microscopy and a Tool for Nanotechnology. *Rev. Sci. Instrum.* **2007**, *78*, 013705.